# Radiation Tolerance of Magnetic Tunnel Junctions With MgO Tunnel Barriers

Fanghui Ren, Albrecht Jander, Pallavi Dhagat, and Cathy Nordman

***Abstract*—The gamma and neutron radiation tolerance of magnetic tunnel junctions with MgO barriers were investigated. The electrical transport and magnetic properties were measured in this effort. The characterization results show no statistically significant change in either tunneling magnetoresistance or coercivity from the radiation.**

***Index Terms*—Coercivity, magnetic tunnel junctions, radiation tolerance, tunnel magnetoresistance.**

## I. Introduction

THE magnetic tunnel junction (MTJ) has attracted enormous attention because of applications in non-volatile magnetoresistive random-access memories (MRAM) and next-generation magnetic field sensors [1]. Semiconductor based circuits and traditional dynamic random-access memories will malfunction or be damaged when exposed to extreme environments, such as space or nuclear radiation [2]–[4]. It is often claimed that since MRAM is based on metallic thin films, it will be less susceptible to radiation effects [5]. However very little experimental evidence regarding radiation tolerance of MTJs has been published. Previous studies on MRAMs mainly focus on the sensitivity of CMOS sense and program circuitry [6]. Determining the radiation tolerance of MTJs, which are the storage elements of MRAMs, is important for investigating their potential application for space and security.

The MTJ consists of two ferromagnetic layers separated by an ultrathin insulating layer, which is referred as the tunnel barrier. The performance of an MTJ significantly depends on the properties of the tunnel barrier, which separates the two adjacent ferromagnetic layers. A previous study on MTJs with an $AlO_x$ barrier shows that the MTJs are not fully radiation hard under intense swift heavy ion bombardments [7]. Recently, there has been a great interest in using MgO as the tunnel barrier, the crystalline nature of which yields giant tunneling magnetoresistance (TMR) ratios due to the interfacial spin-dependent electronic state with $\Delta_1$ symmetry at the Fermi energy [8]. Since the radiation tolerance of MTJs with MgO barrier is unknown, in the present work, we have chosen MgO-based MTJs to conduct the experiment.

Manuscript received July 13, 2012; revised September 23, 2012; accepted September 26, 2012. Date of current version December 11, 2012.

F. Ren, A. Jander, and P. Dhagat are with the School of Electrical Engineering and Computer Science, Oregon State University, Corvallis, OR 97331 USA (e-mail: jander@eecs.oregonstate.edu).

C. Nordman is with the NVE Corporation, Eden Prairie, MN 55344 USA.

Color versions of one or more of the figures in this paper are available online at http://ieeexplore.ieee.org.

Digital Object Identifier 10.1109/TNS.2012.2224375

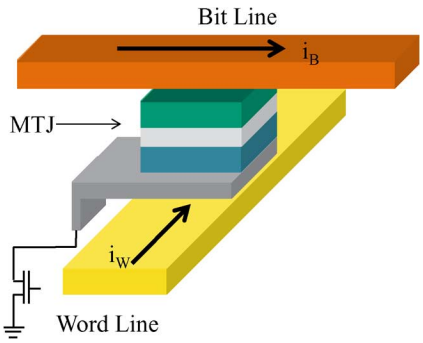


Fig. 1. Schematic diagram of an MRAM cell.

We report the gamma and neutron radiation experiments of the MgO-based MTJs under all the three conditions, i.e. pre-, post-, and during exposure to radiation.

## II. Background

The resistance of the MTJ depends on the configuration of the magnetization of the two ferromagnetic layers, which can be switched separately by an external magnetic field. This phenomenon is called TMR. The spin orientation of the bottom ferromagnetic layer could be pinned by another antiferromagnetic layer via exchange bias, while the top ferromagnetic layers can be switched by the external magnetic field. In MRAM, The antiparallel configuration exhibiting high resistance interprets the binary state 1 and the parallel orientation with low resistance interprets 0. Write pulses passing through the bit line above and word line below are selected to produce the magnetic fields to switch the selected cell, as shown in Fig. 1. During the "write" operation, the transistor is turned on to bias the MTJ. Reading is realized by measuring and comparing the current passing through the MTJ to a reference current by using a two-stage comparator. Among the emerging non-volatile memories, MRAMs possess several assets, such as faster write speeds and unlimited endurance [1].

TMR effect is a consequence of spin-dependent tunneling. The origin of the spin-dependent tunneling can be explained by the difference of Fermi wave vectors for the spin-up and spin-down electrons in ferromagnetic materials due to exchange splitting [9]. As a consequence, tunneling probabilities and tunneling current depend on the relative magnetization of the two ferromagnetic layers, which results in the TMR.

Julliere interpreted the TMR effect in terms of a simple model [10]. In Jullière's model, tunneling current depends on the relative magnetization orientation of the two ferromagnetic electrodes, giving rise to TMR. Jullière's model assumes that spin of electrons is conserved in the tunneling process. The spin-up and

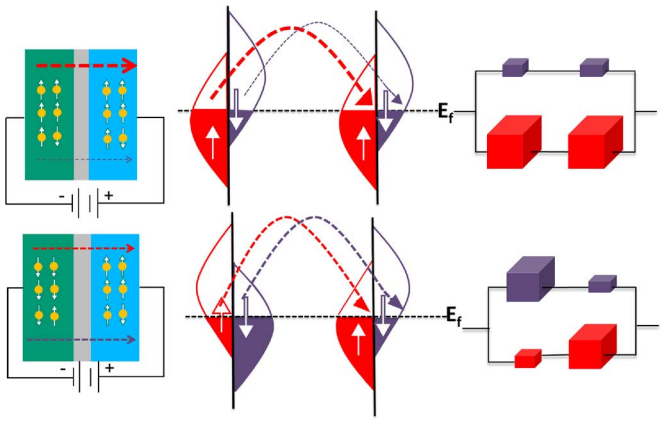


Fig. 2. MTJ characterized by parallel or antiparallel magnetization of the left and right ferromagnetic layers (left panel), the schematic representation of transitions between exchange-split spin bands in the ferromagnetic layers (middle panel), and the equivalent conductance circuit diagram (right panel).

spin-down electrons form a two-spin channel, where electrons can only tunnel into the empty states of the same spin direction. The middle panel in Fig. 2 shows the transitions between exchange-split spin bands in the ferromagnetic layers. If the two ferromagnetic layers are in parallel magnetization, the minority-spin electrons tunnel to the minority states, and the majority -spin electrons tunnel to the majority states. If the layers are magnetized in antiparallel configuration, the majority-spin electrons of the left ferromagnetic layer tunnel to the minority-spin states in the right ferromagnetic layer and vice versa. Jullière's model also assumes that the spin polarization of the tunneling current is determined by the spin polarization of the total electronic density of states of the ferromagnetic layers at the Fermi energy. Since the number of the electrons tunneling within each spin channel can be determined by the density states of spin up and spin down, the tunneling conductance is weighted by the respective spin density of states, as shown in the right panel in Fig. 2. The conductance of parallel (P) and antiparallel (AP) configuration can be written in (1):

$$\begin{aligned} \mathrm{G_P} &\propto \rho_L \uparrow \rho_R \uparrow + \rho_L \downarrow \rho_R \downarrow \\ \mathrm{G_{AP}} &\propto \rho_L \uparrow \rho_R \downarrow + \rho_L \downarrow \rho_R \uparrow \end{aligned} \tag{1}$$

where $\rho_{\mathrm{i}} \uparrow$ and $\rho_{\mathrm{i}} \downarrow$ (i = left or right ferromagnetic layer) represent the tunneling density of states of spin-up and spin-down electrons, respectively.

The spin polarization describes the difference of density of states at the Fermi energy of the ferromagnetic material, as shown in (2):

$$P_i = \frac{\rho_i \uparrow - \rho_i \downarrow}{\rho_i \uparrow + \rho_i \downarrow}. \tag{2}$$

TMR is defined as the difference of conductance between the parallel and antiparallel magnetizations, normalized by the antiparallel conductance, as shown in (3):

$$TMR = \frac{G_P - G_{AP}}{G_{AP}} = \frac{R_{AP} - R_P}{R_P}. \tag{3}$$

Combining (1), (2) and (3), Jullière's model quantifies the magnitude of TMR in terms of the spin polarizations, as shown in (4):

$$TMR = \frac{2P_L P_R}{1 - P_L P_R}. \tag{4}$$

Several factors are important in determining the TMR ratio, including the ferromagnetic materials selection and crystallographic orientation for barrier and ferromagnetic layer. Large TMR values were predicted theoretically for MTJs based on crystalline MgO (001) barrier layers and this prediction was followed by experimental realizations of MTJs using iron and iron alloys as the ferromagnetic materials [8].

The theoretical explanation for a very high TMR ratio obtained by Fe/MgO/Fe sandwich structure relies on the coherent spin dependent tunneling in an MTJ with a crystalline tunnel barrier such as MgO(001) [11]. In 3d ferromagnetic metals and alloys, symmetric $\Delta_1$ Bloch states usually have a large positive spin polarization at $\mathrm{E_F}$, which is desirable for larger TMR. Meanwhile, Bloch states with lower symmetry such as $\Delta_2$ often have a negative spin polarization at $\mathrm{E_F}$. The partial density of states for the decaying evanescent states in the MgO barrier layer indicates that the $\Delta_1$ states have the longest decay length, which results in the slowest decay in the tunnel barrier. However, with an amorphous AlOx barrier, which has no crystallographic symmetry, the momentum of a tunneling electron is not conserved due to scattering within the barrier. This tunneling process can be considered as an incoherent tunneling. Therefore, a large TMR effect in the MTJ with MgO tunnel barrier is expected since $\Delta_1$ electrons dominant tunneling process.

## III. Experimental

MTJs with MgO tunnel barriers were fabricated by magnetron sputtering. The device is a bottom-pinned stack with the full structure being: Si/Ru (60 Å/IrMn (110 Å)/CoFeB(60 Å)/MgO (14 Å)/CoFeB (50 Å), as shown in Fig. 3. Ruthenium acted as the seed layer, the role of which is to improve the texture of the adjacent antiferromagnetic layer. Typically the material used for the antiferromagnetic layer is IrMn. The purpose of this layer is to pin the adjacent magnetic layer via exchange bias to create a spin-valve structure. The tunnel barrier is MgO with (001) crystalline orientation, which is the key to achieving high TMR value. The uniformity and texture of the tunnel barrier heavily influence TMR values. The MgO was deposited from an MgO target by RF sputtering in an oxygen plasma. CoFeB, the ferromagnetic layer, was also deposited by sputtering. After annealing, the amorphous CoFeB layers crystallize to match the MgO orientation, resulting in high orientation in the (001) direction. The devices were patterned using photolithography and the junctions defined by ion milling. The junction areas vary from 1.7 $\mu\mathrm{m}^2$ to 5 $\mu\mathrm{m}^2$.

The experimental and control groups of MTJ samples were prepared by wire bonding to separate printed circuit boards for the tests. Samples in the experimental groups were exposed to gamma and neutron irradiation respectively, while the control groups received no radiation. The control group samples were

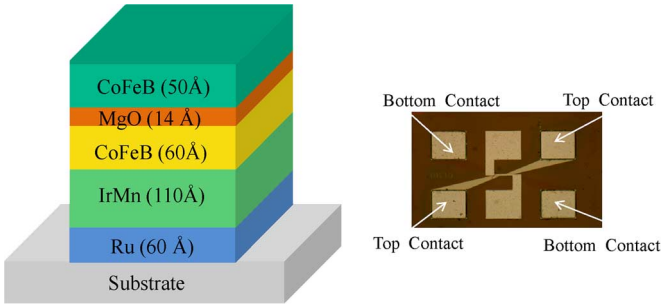


Fig. 3. Illustration of the MTJ stack (left panel) and a die of the MTJ (right panel).

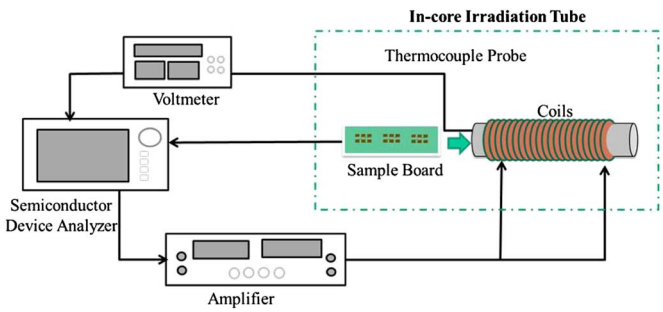


Fig. 4. Experimental setup of neutron radiation test.

subjected to identical handling and thermal cycles. Then the measurements from the control groups were compared to the experimental groups to determine if the radiation had any effect. The devices were characterized by magnetoresistive hysteresis loops and resistance-voltage curves. Four contact pads in a single MTJ die, as shown in Fig. 3, allowed four-terminal measurement of resistance using the Semiconductor Device Analyzer B1500A. The temperature dependence of TMR in all the devices was measured to rule out the effects of temperature variations during the experiments.

The devices in experimental group were characterized before and after exposure to the gamma radiation in Gammacell 220, containing a $^{60}\mathrm{Co}$ source. The dose rate was a constant 9.78 rad/min. The experimental samples initially received a dose of 5.9 Mrad (Si) after which they were again characterized. Irradiation was then continued for a cumulative dose of 10 Mrad, which is significantly greater than the dose typically induces failure of CMOS devices [2], [3]. The devices were re-measured electrically and magnetically.

Neutron radiation experiments were conducted at the Oregon State University TRIGA Mk. II research reactor. The experimental setup is schematically illustrated in Fig. 4. The experimental group devices were characterized *in situ* in a cadmium-lined in-core irradiation tube. Total epithermal neutron fluence up to $2.9 \times 10^{15}/\mathrm{cm}^2$ was obtained, with the flux at $5 \times 10^{10}/\mathrm{cm}^2/\mathrm{s}$ at 50 kW and neutron energies ranging from 0.1 eV to 10 MeV, as shown in Fig. 5.

## IV. Results and Discussions

Figs. 6 and 7 show the characterizations of a single MTJ before and after exposure to the gamma radiation. The hysteresis

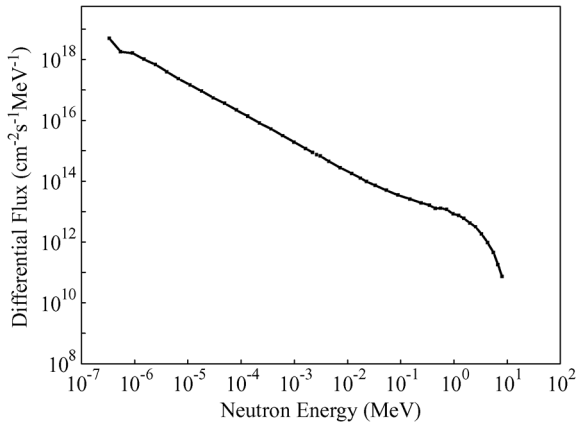


Fig. 5. Neutron spectrum of the cadmium-lined in-core irradiation tube.

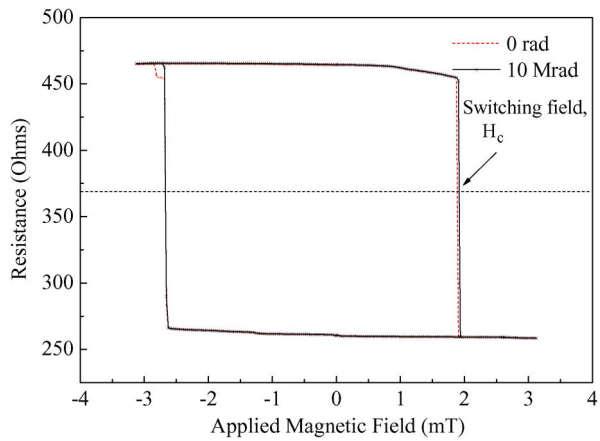


Fig. 6. Hysteresis loop of a single MTJ before and after exposure to the gamma radiation.

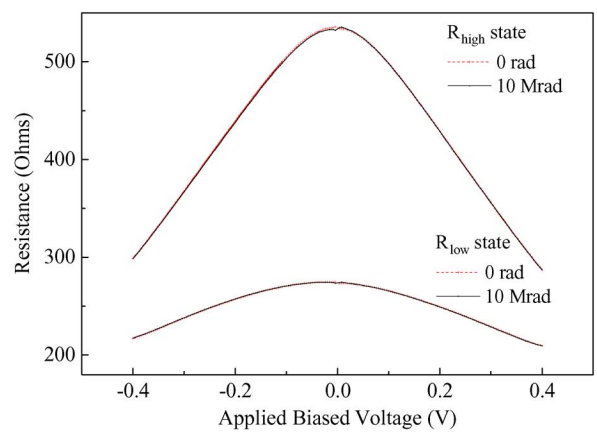


Fig. 7. Voltage bias dependence of the low resistance ($\mathrm{R_{low}}$) state and high resistance ($\mathrm{R_{high}}$) state.

loop and voltage bias dependence of resistance are shown respectively. TMR could be calculated as the resistance difference between the two states normalized by the TMR low resistance.

The measured coercive field $\mathrm{H_c}$ and TMR of the complete series of experimental groups are shown in Figs. 8 and 10, while the control groups are shown in Figs. 9 and 11. The difference in $\mathrm{H_c}$ measured before and after exposure to the radiation is

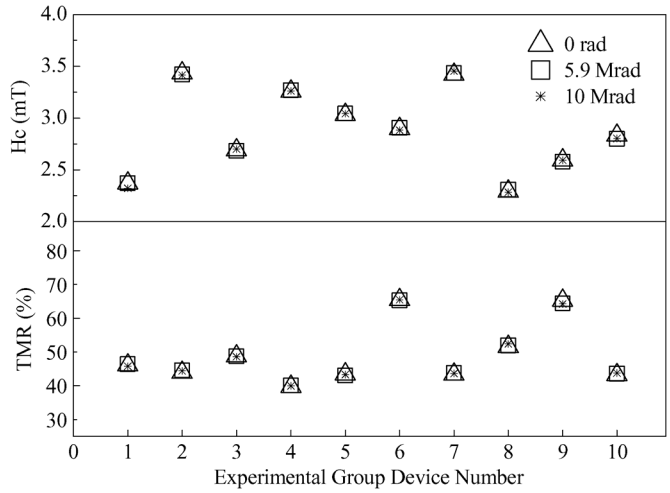


Fig. 8. $H_c$ and TMR of a series of MTJs of the experimental group before and after exposure to the gamma radiation.

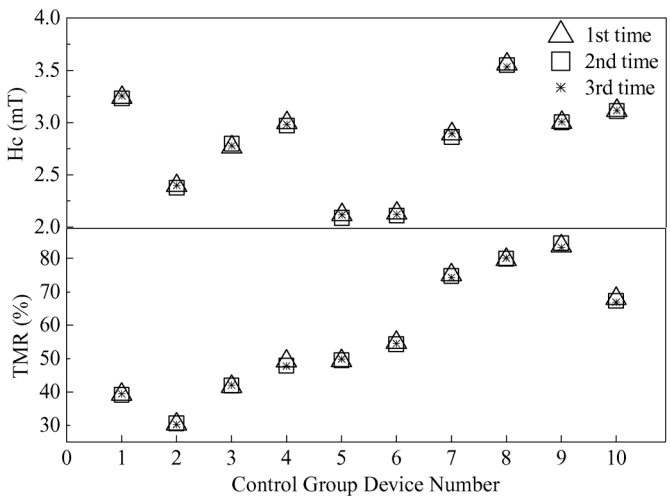


Fig. 9. Characteristics of the control group, which was not irradiated by the gamma radiation.

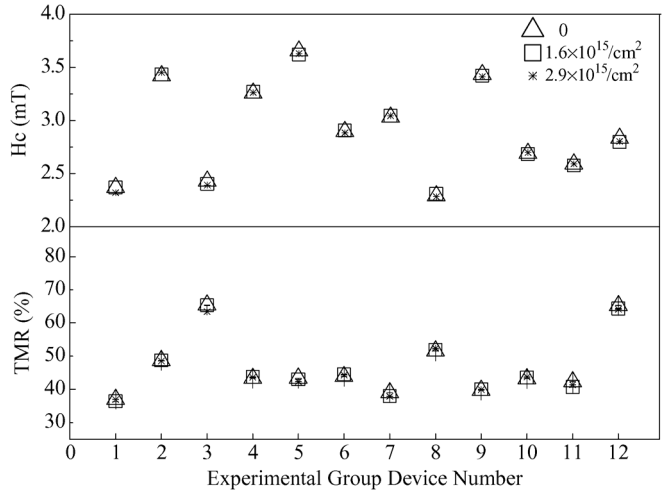


Fig. 10. $H_c$ and TMR of a series of MTJs of the experimental group before and after exposure to the neutron radiation.

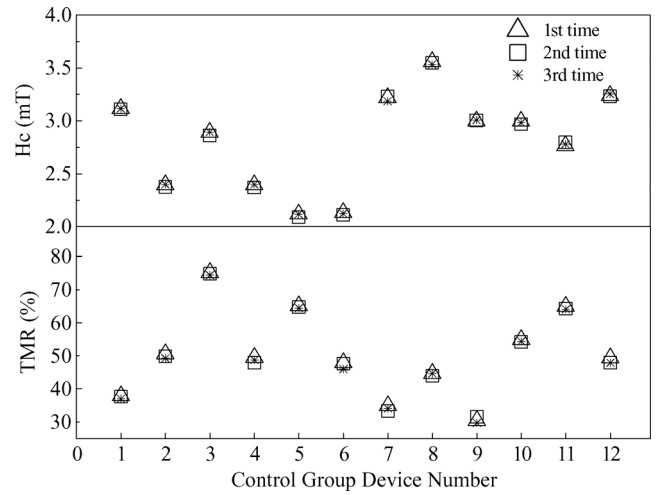


Fig. 11. Characteristics of the experimental group, which was not irradiated by the neutron radiation.

much smaller than the device-to-device variation and insignificant compared to the measurement error. That is, the switching field of the junction devices was not perceptibly affected by the neutron fluence of $2.9 \times 10^{15}/\mathrm{cm}^2$ and accumulated 10 Mrad dose of gamma radiation. After correcting for differences in temperature at the time of testing, the TMR is also found to be unchanged.

For the statistical analysis, we used the Wilcoxon rank sum test to determine whether there were significant differences between the experimental group and control group. Table I shows the statistic test result for the gamma radiation. In the statistic test, the first measurement was set as reference and the relative change of TMR values in the second and the third measurements were calculated. Therefore, two respective statistic tests were required to determine whether the 5.9 Mrad and 10 Mrad doses caused differences. The sample A and B were referred as the two sets of relative change of TMR value in experimental group and control group, respectively. The rank sum results listed in Table I compared with the critical values of the smallest rank sum for the Wilcoxon rank sum test shows that P value is larger than 0.05 [12]. Therefore, it can be concluded that there is no significant statistical difference between the experimental group data and the control group data.

TABLE I
STATISTICAL SIGNIFICANCE TEST FOR THE GAMMA RADIATION

| Statistic Test | Rank Sum of Sample A (Experiment Group) | Rank Sum of Sample B (Control Group) |
|---|---|---|
| Test 1 | 90 | 120 |
| Test 2 | 93 | 117 |

Ionization damage is the dominant mechanism of interaction of energetic photons (gamma radiation) with CMOS devices [13]. On the other hand, due to the much higher carrier concentration in metal-based MTJs, the ionized carriers have an insignificant effect on the transport properties. No effect on the magnetic properties of the MTJs was observed upon radiation. Soft magnetic metals and alloys have structure that is insensitive to epithermal neutron radiation [14], [15].

## V. Conclusion

Neither the electrical nor the magnetic properties of MTJs were affected by the radiation. It has been determined that MgO-based MTJs are highly tolerant of gamma radiation, particularly in comparison to silicon field-effect transistors which have been shown to degrade with gamma ray exposure even as low as 100 Krad [16], [17]. Moreover, the MTJs are insensitive to the epithermal neutron fluence of $2.9 \times 10^{15}/\mathrm{cm}^2$, a dose which could cause irreversible displacement damage in silicon dioxide and high k semiconductor materials [18].

## References


[1] W. J. Gallagher and S. P. Parkin, "Development of the magnetic tunnel junction MRAM at IBM: From first junctions to a 16-Mb MRAM demonstrator chip," *IBM J. Res. Develop.*, vol. 50, pp. 5–23, Jan. 2006.

[2] P. E. Dodd, "Current and future challenges in radiation effects on CMOS electronics," *IEEE Trans. Nucl. Sci.*, vol. 57, pp. 1747–1763, Aug. 2010.

[3] F. P. Korshunov, "Radiation effects in bipolar and CMOS integrated microcircuits," in *Proc. 2008 18th Int. Crimean Conf. Microwave and Telecommunication Technology*, pp. 15–16.

[4] H. L. Hughes and J. M. Benedetto, "Radiation effects and hardening of MOS technology: Devices and circuits," *IEEE Trans. Nucl. Sci.*, vol. 50, pp. 500–520, Jun. 2003.

[5] S. Gerardin and A. Paccagnella, "Present and future non-volatile memories for space," *IEEE Trans. Nucl. Sci.*, vol. 57, pp. 3016–3039, Dec. 2010.

[6] J. Heidecker and G. Allen, "Single event latchup (SEL) and total ionizing dose (TID) of a 1 Mbit Magnetoresistive Random Access Memory (MRAM)," presented at the 2010 IEEE Radiation Effects Data Workshop (REDW), 2010.

[7] Y. Conraux and J. P. Nozie'res, "Effects of swift heavy ion bombardment on magnetic tunnel junction functional properties," *J. Appl. Phys.*, vol. 93, pp. 7301–7303, May 2003.

[8] S. Yuasa, "Giant tunneling magnetoresistance in MgO-based magnetic tunnel junctions," *J. Phys. Soc. Jpn.*, vol. 77, p. 031001, Mar. 2008.

[9] E. Y. Tsymbal, O. N. Mryasov, and P. R. LeClair, "Spin-dependent tunnelling in magnetic tunnel junctions," *J. Phys. Condens. Matter*, vol. 15, pp. R109–R142, Feb. 2003.

[10] M. Julliere, "Tunneling between ferromagnetic films," *Phys. Lett. A*, vol. 54, pp. 225–226, Sept. 1975.

[11] J. Mathon and A. Umerski, "Theory of tunneling magnetoresistance of an epitaxial Fe/MgO/Fe(001) junction," *Phys. Rev. B*, vol. 63, p. 220403, May 2001.

[12] C. Cleaeys and E. Simoen, *Radiation Effects in Advanced Semiconductor Materials and Devices*. New York: Springer, 2002, pp. 12–13.

[13] G. K. Kanji, *100 Statistical Tests*. London, U.K.: SAGE, 1993, pp. 218–219.

[14] D. I. Gordon and R. S. Sery, "Effects of charged particles and neutrons on magnetic materials," *IEEE Trans. Nucl. Sci.*, vol. 10, pp. 20–27, Nov. 1963.

[15] A. Dunlop, D. Lesueur, and P. Legrand *et al.*, "Effects induced by high electronic excitations in pure metals: A detailed study in iron," *Nucl. Instrum. Meth. B.*, vol. 90, pp. 330–338, May 1994.

[16] Z. Hu, Z. Liu, H. Shao, Z. Zhang, B. Ning, M. Chen, D. Bi, and S. Zou, "Comprehensive study on the total dose effects in a 180-nm CMOS technology," *IEEE Trans. Nucl. Sci.*, vol. 58, pp. 1347–1354, Jun. 2011.

[17] H. L. Hughes and J. M. Benedetto, "Radiation effects and hardening of MOS technology: Devices and circuits," *IEEE Trans. Nucl. Sci.*, vol. 50, pp. 500–520, Jun. 2003.

[18] J. R. Srour, "Review of displacement damage effects in silicon devices," *IEEE Trans. Nucl. Sci.*, vol. 50, pp. 653–670, Jun. 2003.